PNC-TN941 83-26

Sodium Boiling Experiment in a 37-Pin Bundle under Loss-of-Flow Conditions

February, 1983

OARAI ENGINEERING CENTER

POWER REACTOR AND NUCLEAR FUEL DEVELOPMENT CORPORATION

動力炉・核燃料開発事業団（Power Reactor and Nuclear Fuel Development Corporation）

PNC-TN941 83-26
Feb, 1983

The Tenth Meeting of the Liquid Metal Boiling Working Group,
Karlsruhe, October 27-29, 1982

Sodium Boiling Experiment in a 37-Pin Bundle under Loss-of-Flow Conditions

K. Haga

FBR Safety Engieering Division,
O-arai Engineering Center, Power Reactor and Nuclear Fuel Development Corporation
4002 Narita, O-arai, Ibaraki-ken, 311-13, Japan

ABSTRACT

A series of loss-of-flow experiments was conducted in an electrically heated 37-pin bundle which simulated a MONJU fuel subassembly. The flow was reduced exponentially by a pump power control system. The radial temperature profile at boiling inception showed a trapezoidal shape independent of the flow decay curve and heat flux.

Boiling initiated at the top end of the heated section, then the bubble expanded mainly to the upstream central subchannels and to the downstream unheated section according to the expansion of the saturated temperature region. When the voided zone covered the whole flow cross-section, the growth and collapse of a piston-like bubble repeated and the inlet flow decreased rapidly keeping the oscillation expanding.

Dryout occurred when the flow oscillation became large enough to cause temporary flow reversal. Although reentry of the liquid slug rewetted the dried pin surfaces, the subsequent flow reversal caused dryout again.

1. Introduction

One of the typical hypothetical accident initiators of LMFBRs is the loss-of-flow without scram. Many experimental studies have been conducted in this field including those with bundle geometries. However, previous experimental information is not enough, especially in large bundle sizes, for the investigation of void behavior in fuel subassemblies and its relation to dryout. It is said that a trapezoidal temperature profile is formed across a fuel subassembly due to the existence of the cold peripheral subchannel ring. The closer the subchannel is to the center, the smaller the influence of outermost subchannels. For this reason experimental data with a larger bundle which has a long heated region is favorable to predict the phenomena in actual fuel subassemblies [1].

The present experimental study was performed using a 37-pin bundle for the above mentioned objectives, that is, to obtain the data on void pattern transition and on the dryout condition during the loss-of-flow accident.

2. Test section

The experiments were carried out using the Sodium Boiling and Fuel Failure Propagation Test Loop, SIENA, at the O-arai Engineering Center, Power Reactor and Nuclear Fuel Development Corporation (PNC). A description of the SIENA is given in Ref. [2]. The test section named "37F" is shown in Fig. 1. The bundle consisted of 37 electrically heated pins. Tantalum was used as the heating element in the pins. The electrical resistance of tantalum changs with the temperature such that the maximum heat flux under boiling conditions was higher than the mean axial heat flux by 10 to 20 %. Unfortunately, because one heater pin failed in a preliminary run, all boiling runs were conducted with heating in the remaining 36 pins. Each pin 6.5 mm in diameter was wrapped by a 1.3 mm diameter spacer wire with a 264.8 mm helical pitch. The diameters and the pin pitch of 7.9 mm were of the same configuration with MONJU fuel subassemblies. The bundle had a 450 mm heated length and a 715 mm simulated fission product gas plenum at the top end. The 37 pins were installed in a hexagonal Inconel-600 tube of 10 mm thickness so that the gap between the peripheral pins and the inner duct wall was 1.45 mm. Thermal insulation on the outer wall of the hexagonal tube minimized heat losses through the duct wall.

Chromel-Alumel thermocouples 0.3 mm in diameter were embedded in the outer surfaces of pin sheaths at 10 cross sections, which were named alphabetically from A to J. The subchannel temperature measurements were made by the 0.3 mm diameter thermocouples whose hot juctions were located at the subchannel centers, and by several spacer wires made of 1.3 mm-diameter thermocouples. The test section inlet and outlet temperatures and outer duct wall temperatures were monitored by additional thermocouples.

Two types of void-meters were used to detect voids. A total of 14 resistance void-meters was attached to the duct wall to detect the volume averaged void fraction. In addition, 10 Chen-type void-probes located in the spacer wires were used to detect local voids. Pressure transducers and electromagnetic flow-meters were provided at the inlet and outlet of the test section. Output signals from the above sensors were recorded using a digital data acquisition system controlled by an HP-2116C computer.

3. Operating procedures

Prior to the experiments, the oxygen concentration of the sodium was controlled by a purification system to below 10 ppm.

Two series of experiments have been conducted. The first was the single -phase flow heat transfer test, which was designed to examine the reference steady temperature profiles for the analysis of subsequent LOF experiments.

These runs were performed under the following conditions:

Flow velocity:	0.53-4.88 m/s
Inlet temperature:	272-293 °C
Heat flux:	3.6-42.0 W/cm^2

The second series was the LOF boiling experiments, in which transient boiling phenomena were investigated. The experiments were performed in the following manner. The inlet temperature and the cover gas pressure were regulated and by-pass lines were closed to supply high flow to the test section to attain the same flow velocities as in a fuel subassembly at the normal operating condition. Thereafter, the supply voltage, E, of the electromagnetic pump in the main line was reduced exponentially by a control circuit which was especially made for these experiments.

$$E_0 = (E_0 - E_{terminal}) \exp(-t/a) + E_{terminal}$$

where E_0 is the initial voltage to the pump, $E_{terminal}$ is the terminal voltage, a is a time constant and t is the transient time.
Thirty four runs were conducted. The experimental conditions are summarized as follows:

Inlet temperature	453-530 °C
System pressure at the top of heated section	1.21×10^5 - 1.69×10^5 Pa
Initial flow velocity	3.54, 5.10-5.24 m/s
Time constant for flow coastdown curve	3-20 s
Time before boiling inception	12-103 s
Flow velocity at inception of boiling	0.23-0.26, 0.67-0.77 m/s
Average heat flux in boiling	34.3-44.9, 71.3-79.4 W/cm^2

4. Results and discussion

4.1. Temperature profile under steady non-boiling conditions

Figure 2 shows the typical results of steady non-boiling runs. The radial coolant temperature profiles at Section G, i.e. at X = -11.3 mm, are shown. Here, X denotes the distance from the top end of the heated zone and its negative sign means that the cross-section is upstream from the end. Run 37H-260-2 is chosen from high flow cases and Run 37H-30-2 from low flow cases.

The temperature profiles of both runs are almost identical and have steep slopes in the outer subchannels. There has been concern that under LOF conditions these trapezoidal shapes could not be maintained, as was observed in our 19-pin bundle experiment [3], due to the duct wall which may work as a heat sink.

4.2. Radial temperature profile at boiling inception

Boiling was initiated with relatively low superheat (less than 50 °C) [4]. Figure 3 shows the radial temperature profiles at Section G before flow coastdown and at boiling inception in two runs, i.e. 37FC-21 and 37FC-32. Although the two runs differ widely in heat flux, the terminal pump power and the time into boiling inception, the temperature profiles at boiling inception were almost identical, viz, a flat temperature region was formed in the first and second subchannel rings from the bundle center and the temperature differences between the inner subchannels and the outermost subchannels were about 120°C. Figure 4 compares the temperature profile data obtained in three other runs with different time constants for flow coastdown curves, i.e. 37FC-30, 32, and 34. The shapes are similar as those shown in Fig. 3. It was found from these figures that at boiling inception a flat saturation temperature region was formed in the center of the bundle as in a fuel subassembly. The remaining difference which affects the boiling behavior, between 37F and the actual subassembly is the flow area ratio of subcooled outer subchannels to the whole cross-section. The transient temperature differences between the central and the peripheral subchannels in a full subassembly may be estimated from the data of the present experiments.

4.3. Dynamic boiling behavior in multi-pin geometry

In this series of experiments, almost all runs were terminated by power shutdown at inception of flow reversal to keep the integrity of the bundle. Run 37FC-34 was the only run in which the pin power was maintained

until the occurrence of dryout. The records of the run are explained below.

Temperature and inlet flow changes

Figure 5 shows the signals of temperature at Section G and the inlet flow-meter. The experimental conditions of Run 37FC-34 were: initial steady-state flow velocity, 5.24 m/s; inlet temperature, 530 °C; system pressure at the top end of the heated region, 1.71×10^5 Pa; average heat flux at steady state, 88.8 W/cm^2; average heat flux in boiling, 74.4 W/cm^2; and maximum axial heat flux in boiling, 80.3 W/cm^2. The horizontal axis in the figure shows the relative time from the start of flow coastdown. The pump power control system caused small oscillations during the flow transient. When the inlet flow velocity decreased to 0.67 m/s at 14 sec, the pin surface temperatures in the central subchannels, T-101G and T-203G, reached the sodium saturation temperature and boiling initiated. The temperature T-306G in the third subchannel ring joined the saturation temperature level soon thereafter. However, the outermost subchannel ring had such a low temperature ramp rate that it took 26 seconds until T-408G showed saturation. It can be considered that the voided region covered the whole cross-section at this moment. Also, the amplitude in the inlet flow signal oscillation began to increase at the same moment. Thereafter a rapid decrease in the inlet flow rate was also identified. These inlet flow changes were due to the additional pressure loss in the bundle caused by the void that expanded and occupied the whole cross-section.

The reversal of flow repeated several times and the absolute values of the peak reverse flow increased each time. Meanwhile the temperature oscillations which corresponded to the saturation pressure change began to deviate from the saturation temperature. Temporary dryout must have caused the high temperature measurement. When the temperature exceeded 1000 °C, the pin power was cut off automatically by the safety circuit.

Figure 6 shows the pin surface temperature changes at an upstream location, Section D (X = -143.8 mm). The temperature in the central subchannel reached the saturation point at 26 sec, then the ramp rates of the outer subchannel temperatures were increased. A steep temperature rise beyond 1000 °C was measured also at this cross section.

Void signals

Outputs of the Chen-type void-meters, C-09 and C-10, located at Section H (X = 55.0 mm) are shown in Fig. 7. Void-meters are so sensitive to the temperature change that the strange signals are generated markedly during such transient states. The void in the early boiling stage is recognized by signal spikes. The radial expansion of the voided region can be discerned from the data that a void was detected earlier by C-09 located inside C-10. After 18 sec, one can easily identify whether the sensor tips were occupied by liquid or void, and the signals from C-09 and C-10 became coherent. This means that the bubble behaved in the same manner over the cross-section, that is, one-dimensionally. A chain of rectangular signals after 26 sec is due to the passing of liquid slugs though the Section H with relatively regular intervals.

Figure 8 shows the records of resistance void-meters VoT-9 and VoT-10, which give outputs corresponding to the averaged void fractions over the 50 mm long axial sections located at X = 50 to 100 mm and X = 100 to 150 mm, respectively. The remarkable coherence of the timing of void detection by two types of sensors (VoT-9 and C-09, C-10) confirms the one-dimensional void behavior as was observed in our single-pin experiment[5].

Summarizing the results of these void-meters signals, the following can be said about the thermodynamics under loss-of-flow conditions. Initially,

a void is formed at a central region, then it expands radially and axially. During this time period, the inlet flow decrease is slight. After the void region occupies the whole cross-section, the void pattern changes into a one-dimensional mode. The void repeats an expansion and contraction behavior. The increased pressure loss in the bundle further decelerates the inlet flow. Eventually, the flow reversal occurs.

Saturation temperature and voiding boundary behavior

Figure 9 shows the saturation temperature region boundaries at G and H sections in Run 37FC-34. The deformation of the boundary from a circle is probably due to the existence of an unheated pin. These maps can be obtained at any moment during boiling, but it is impossible to express them all in one figure. In addition, the cross-sections which have enough themocouples to draw such figures were limited. Thus instead of figures at each section, the overall saturation temperature movements in the test section are shown two-dimensionally in Fig. 10. In this figure, the circumferential locations of thermocouples in the bundle are neglected, and the time when the thermocouples showed the saturation temperature was averaged in every subchannel ring considering the volume weight of the location of the thermocouples. In the figure those regions with less shading grade, correspond to the locations where more subchannel rings are covered by saturated coolant. The information from the void-meters was also added in this figure. It is reasonable that the data from Chen-type void-meters qualitively agree with the saturation temperature map. Conversely it can be said that the region where voids exist is identical with the saturation temperature region. The lanky sinusoidal lines appearing in the latter half of boiling duration time were drawn from the signals of the resistance void-meters. It is interesting that the envelopes of the sinusoidal lines seem to agree with the timing when the whole cross-section is covered by the saturated coolant.

Dryout phenomena

Figure 11 shows the records of inlet flow-meter F-103, outlet flow-meter F-107, resistance void-meter VoT-7, pressure transducers P-108, P-109 and thermocouples T-204G and T-101G in the last stage of Run 37FC-34. The pressure spikes observed periodically are due to bubble collapse. Initially the thermocouples showed the saturation temperature corresponding to the changing pressure even if the pin surface had been covered by sodium vapor for about one second. Then T-204G began to show a rapid increase which was interrupted by rewetting. This process was repeated. The dryout duration time coincided with the time between two events. One of them is that the outlet flow-meter showed zero value, which means that the upper end of the void boundary stood still under the flow-meter location or passed beyond the point. The another event is that the inlet and outlet flow-meters took peak values of opposite signs, which means that the bubble was being compressed rapidly. The timing of rewetting shown by T-204G is a little earlier than the time when the void-meter detected a void. Sodium droplets or mist in the vapor phase must have deposited on the pin surface before liquid coolant washed the surface again. The dryout duration time became longer with the repetition of dryout. Thus the temperature will become higher, and will ultimately exceed the cladding melting point.

Dryout mechanism

As the mechanism of dryout, the liquid film evaporation model from the

pin surface is often used in computer codes such as in the SAS [6] series. If a stationary film is assumed, the thickness of the liquid film left on the pin surface in the process of void expansion can be calculated from the time interval between two events: from the appearance of void covering the heating surface to the dryout occurrence. Trial calculations yielded film thicknesses of 0.053 mm, 0.061 mm, and 0.033 mm for the first, second, and third dryout, respectively. Özgü and Chen [7] reported from their gas slug expulsion experiment in a water column that the minimum residual liquid film thickness is 0.015 multiplied by the hydraulic diameter. This value for 37F is 0.051 mm, which is close to the above calculated ones. However, the fact that no pin surface showed a temperature excursion before 19.4 sec, even if it was covered by a void for about one second and also the fact that dryout ceased before the pin surface was covered by the liquid column as shown in Fig. 11, would not support the residual liquid film model for dryout. Thus, a new concept must be considered on the dryout mechanism.

An idea that the mist flow in the voided zone prevents dryout of the pin surface is proposed by our low flow-low heat flux boiling [8] and local boiling exepriments [9]. This assumption seems also consistent with the present test results. The amount of liquid deposition on the heating surfaces will be so small, however, that to avoid the heat removal crisis, the droplet or mist must always flow over the pin surface in the voided zone. The mist flow will temporarily disappear in the one-dimensionally expanded and stagnated void region before the void begins the contraction process. This situation will cause temporary dryout. Hence flow reversal or almost stagnant flow would take place before dryout occurrence. This event sequence itself does not contradict SAS calculational results [10]. Furthermore the cooling capability of mist in the voided zone is promising to make the accident progress milder than that calculated by codes which do not include this effects.

5. Conclusions

Transient sodium boiling experiments were conducted using a 37-pin bundle under loss-of-flow conditions. Changes in temperature, flow velocity, pressure and void were measured during the transients. The following conclusions were drawn concerning boiling phenomena.

1. The void behavior is summarized below.
   (1). The bubble was formed at the end of the heated zone at first, then it expanded mainly toward the upstream central subchannels and toward the downstream unheated zone, and then in the radial direction according to the expansion of the saturated temperature region.
   (2). When the bubble covered a whole flow cross-section, the inlet flow reduction was accelerated.
   (3). The inlet and outlet flow velocities oscillated violently due to the growth and collapse of a piston-like bubble, and inlet flow reversal was observed.
2. Dryout of pin surfaces occurred after the inception of flow reversal. Dryout ceased because of pin rewetting, but it took place again in the next flow reversal. This sequence was repeated several times. Gradually the dryout region expanded and the pin surface experienced higher temperatures.
3. A dryout mechanism was proposed. It leads to the conclusion that the disappearance of liquid droplet or mist flow in the voided zone causes the heat removal crisis.

Data obtained from these experiments are being used for the model development and its verification of the computer codes for accident analysis.

Acknowledgment

The author is indebted to Messrs. T. Isozaki, T. Komaba, M. Uotani, K. Sahashi, K. Yamaguchi and Y. Kikuchi for their engineering and technical contributions throughout the experiments. The author particularly wish to express his thanks to Dr. C. L. Larson for his assistance in manuscript preparation.

References

[1] R. Nijsing and W. Eifler, "Considerations on Incoherency of Boiling and Voiding in LMFBR Subassemblies during a Loss-of-Flow Accident," Proceedings of the ENS/ANS Topical Meeting on Nuclear Power Reactor Safety, pp.735-746, Brüssel, 1978.

[2] K. Yamaguchi et al., "Experimental Investigation of Local Cooling Disturbances in LMFBR Fuel Subassemblies," ASME Winter Annual Meeting, 81-WA/HT-40, 1981.

[3] Y. Kikuchi and K. Haga, "Sodium Boiling Experiments in a 19-pin Bundle under Loss-of-Flow Conditions," Nucl. Eng. and Design, Vol. 66, 1981, pp.357-366.

[4] A. Ohtsubo and K. Haga, "Incipient Sodium Boiling Superheats in Bundle Geometry under Loss-of-Flow Conditions," J. Nucl. Sci. Technol. (submitted for publication).

[5] Y. Kikuchi and K. Haga, "Transient Boiling of Sodium in a Single-pin Geometry under Loss-of-Flow Conditions," J. Nucl. Sci. Technol., Vol. 15, 1978, pp.100-108.

[6] F. F. Dunn et al, "The SAS2A LMFBR Accident Analysis Computer Code," ANL-8138, 1974.

[7] R. Özgü and J.C. Chen, "Local Film Thickness During Transient Voiding of a Liquid Filled Channel," ASME Winter Annual Meeting, 75-WA/HT-27, 1975.

[8] K. Haga et al., "Decay Heat Removal under Boiling Condition in a Pin-Bundle Geometry," Proceedings of the 9th Liquid Metal Boiling Working Group Meeting, Rome, 1980.

[9] K. Yamaguchi et al., "Boiling and Dryout Conditions in Disturbed Cluster Geometry and Their Application to the LMFBR Local Fault Assessment," to be presented at the 2nd International Topical Meeting on Nuclear Reactor Thermalhydraulics, Santa Barbara, January 1983.

[10] Edited by H. Fenech, "Heat Transfer and Fluid Flow in Nuclear Systems," pp.287-298, Pergamon Press, 1981.

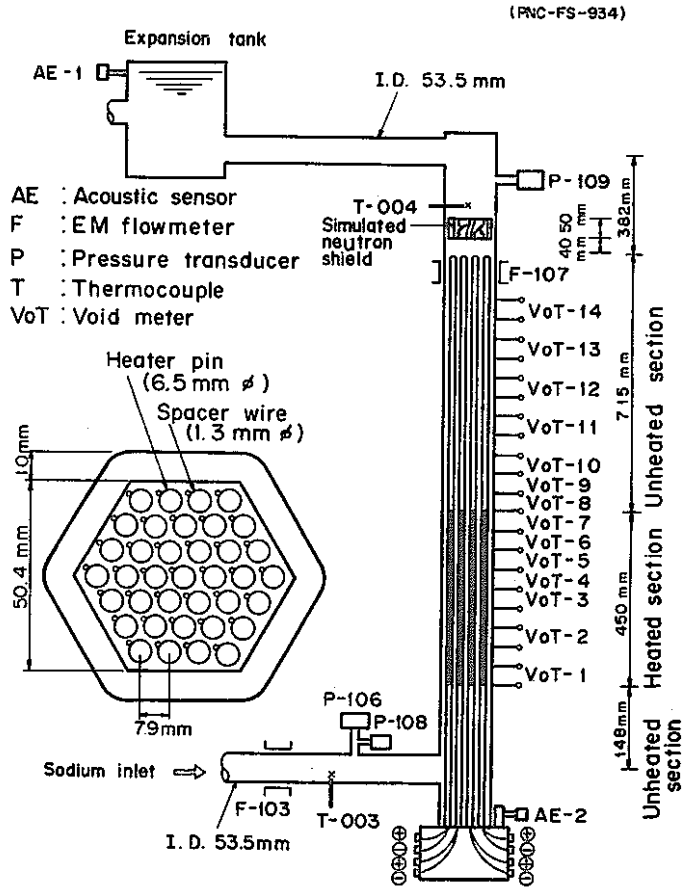

Fig. 1 37-pin bundle test section (37F)

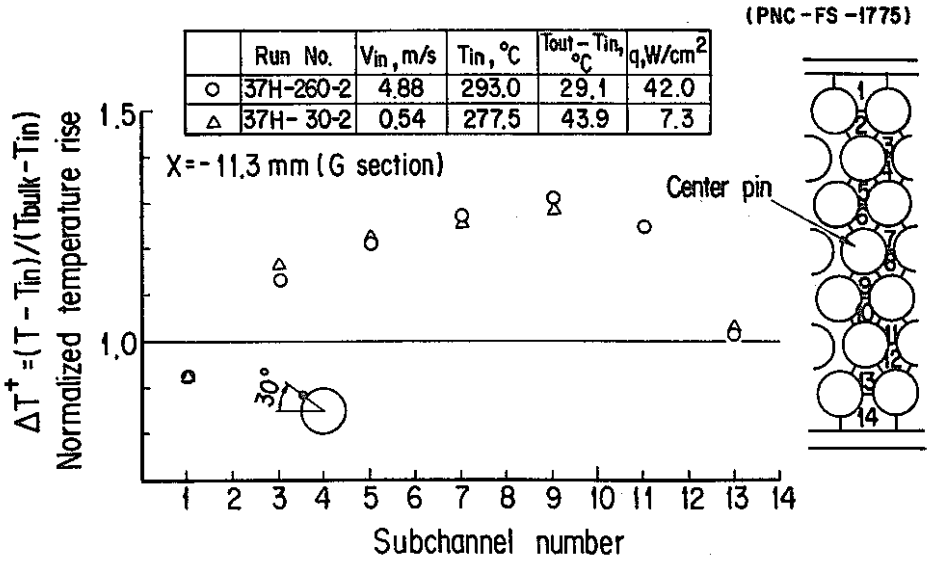

Fig. 2 Radial temperature profiles in steady single-phase tests

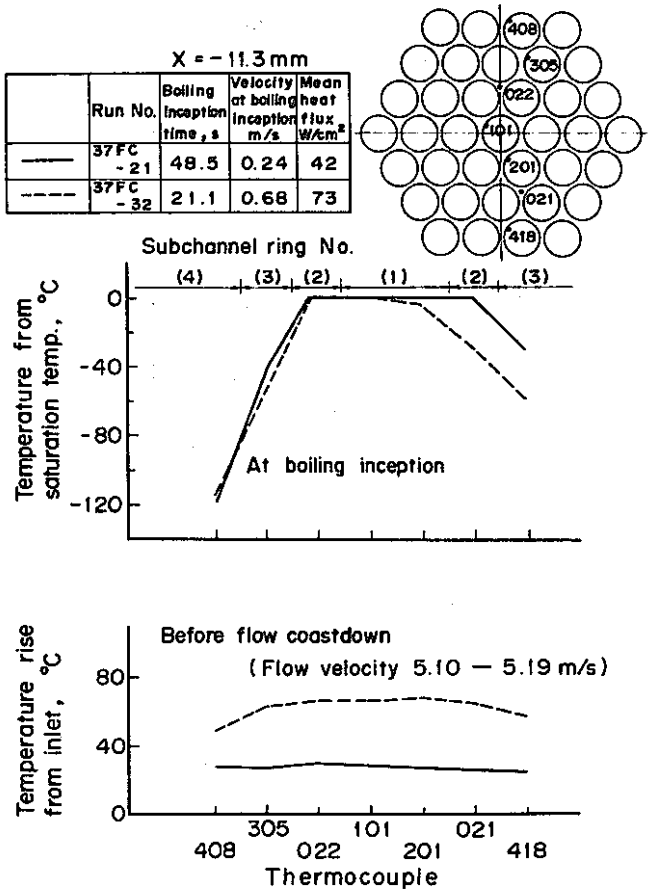

Fig. 3 Radial temperature profiles at boiling inception, Runs 37FC-21 and 37FC-32

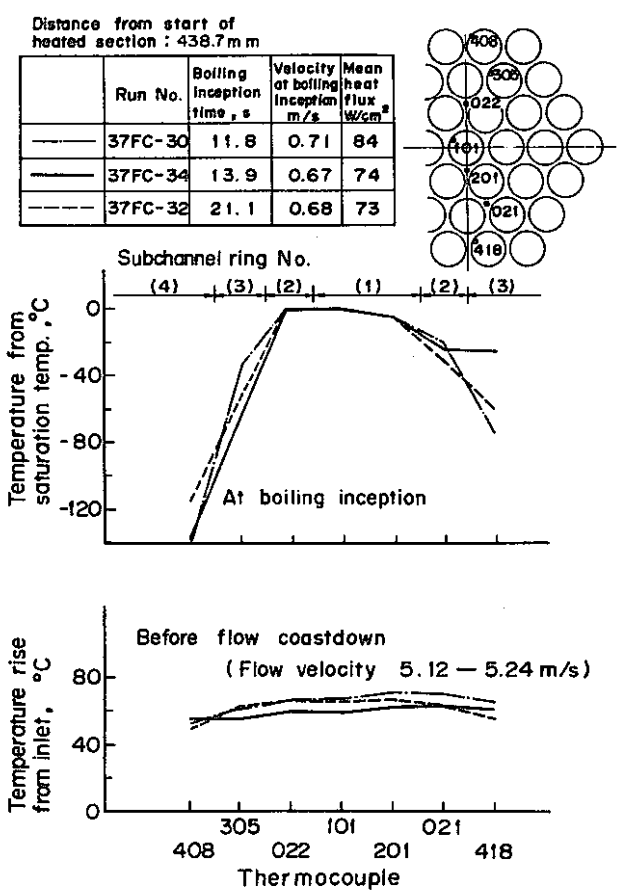

Fig. 4 Radial temperature profiles at boiling inception, Runs 37FC-30, 37FC-32 and 37FC-34

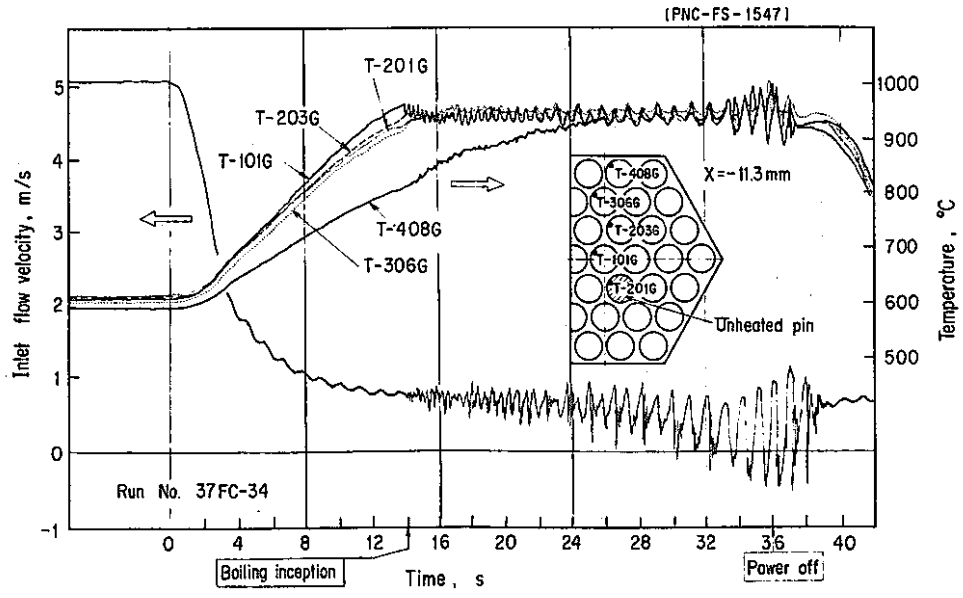

Fig. 5 Temperature signals at Section G

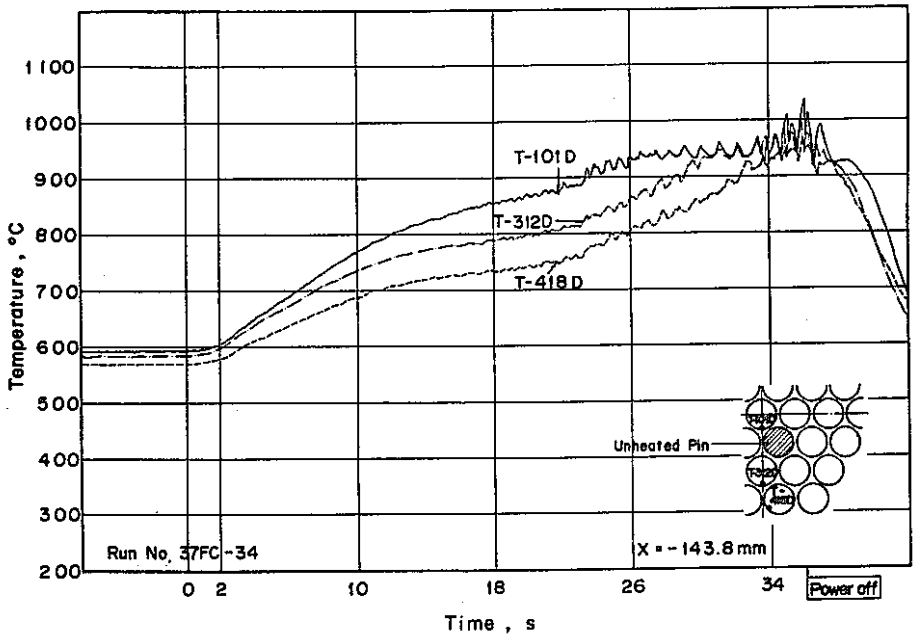

Fig. 6 Temperature signals at Section D

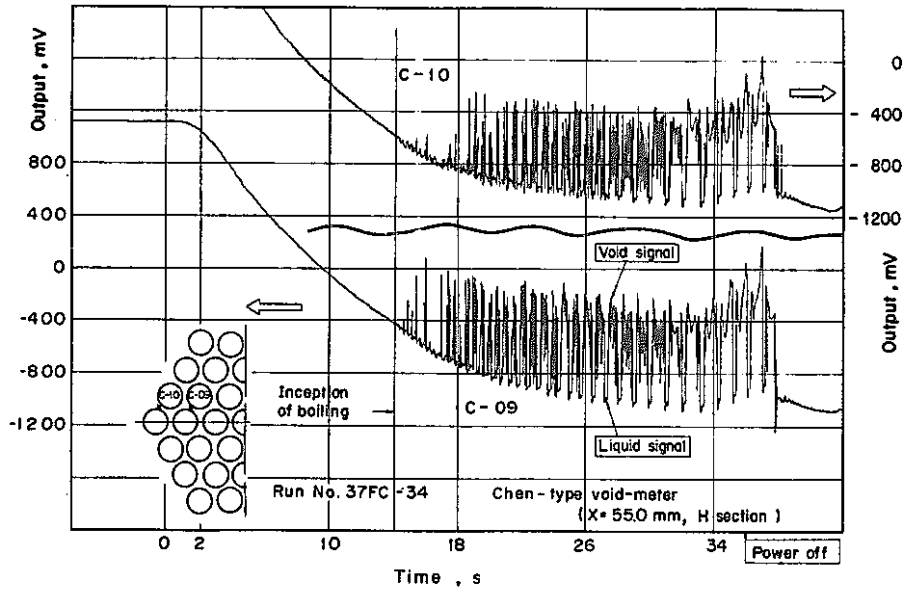

Fig. 7 Chen-type voidmeter signals

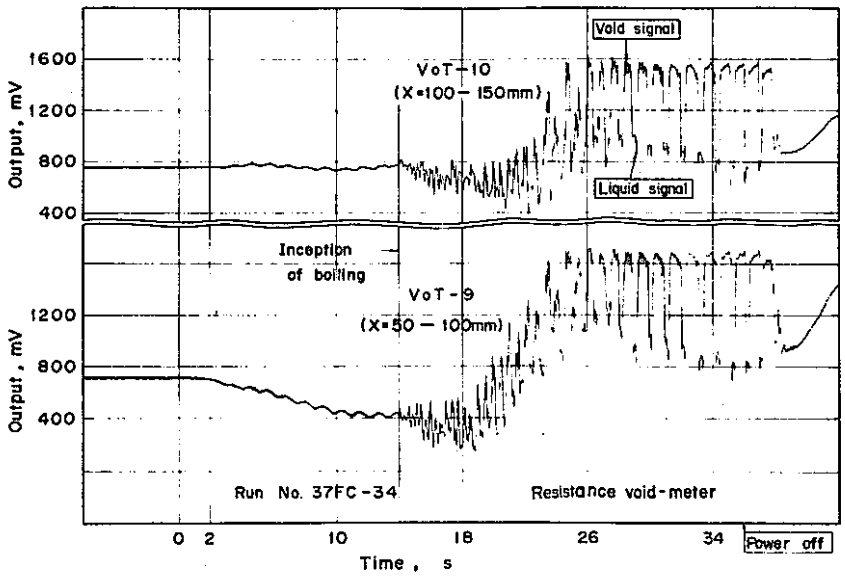

Fig. 8 Resistance void-meter signals

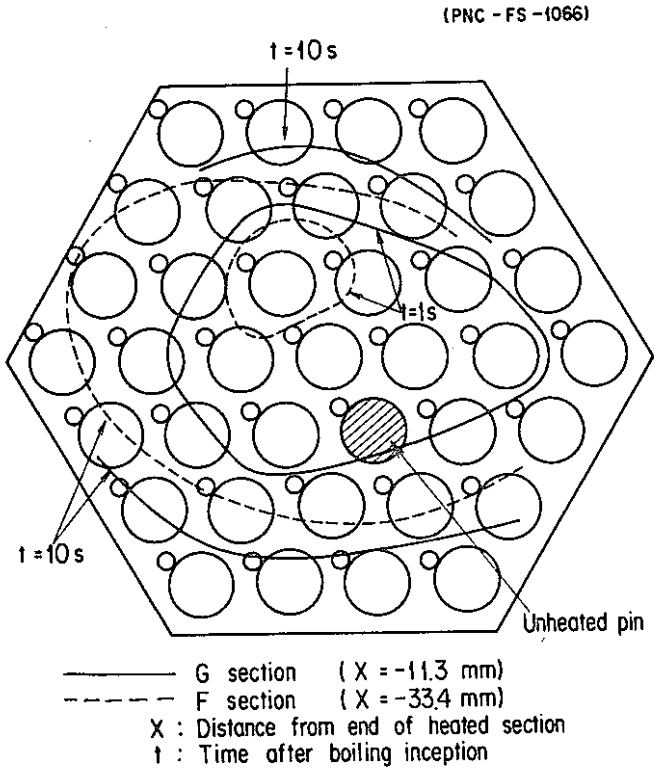

Fig. 9 Expansion of saturated temperature region at G and F sections

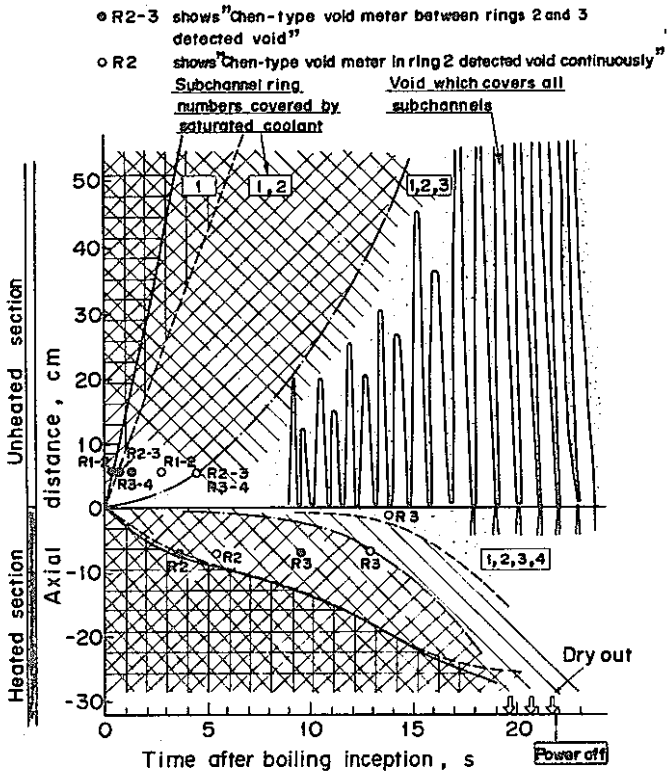

Fig. 10 Axial movement of saturation temperature boundary

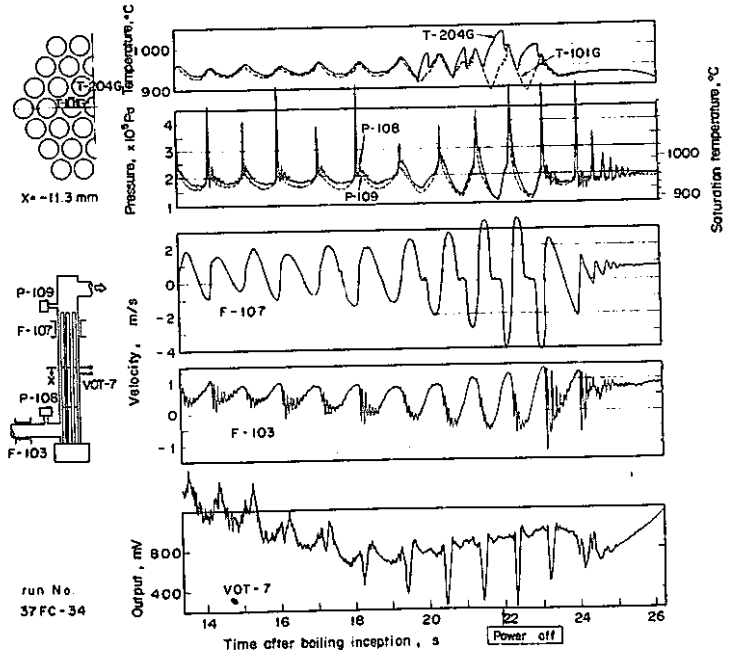

Fig. 11 Signals of temperature, pressure, flow and void at the end of Run 37FC-34